Briefings in Bioinformatics, 2024, **25(5)**, bbae401
https://doi.org/10.1093/bib/bbae401
Case Study

A computational approach to developing a multi-epitope vaccine for combating *Pseudomonas aeruginosa*–induced pneumonia and sepsis

Suronjit Kumar Roy[1,‡], Mohammad Shahangir Biswas[1,2,*,‡], Md. Foyzur Raman[1], Rubait Hasan[1], Zahidur Rahmann[3], Md Moyen Uddin PK[4]

[1]Department of Biochemistry and Biotechnology, Khwaja Yunus Ali University, Chouhali, Sirajganj 6751, Bangladesh
[2]Department of Public Health, Daffodil International University, Birulia, Dhaka 1216, Bangladesh
[3]Riceland Healthcare, 538 Broadway Ave, Winnie, TX 77665, United States
[4]Institute of Biological Science, Rajshahi University, Motihar, Rajshahi 6205, Bangladesh

*Corresponding author. Department of Biochemistry and Biotechnology, School of Biomedical Science, Khwaja Yunus Ali University, Enayetpur, Sirajgonj 6751, Bangladesh. E-mail: bioshahangir@gmail.com

‡Suronjit Kumar Roy and Mohammad Shahangir Biswas contributed equally to this work and should be considered co-first authors.

Abstract

Pseudomonas aeruginosa is a complex nosocomial infectious agent responsible for numerous illnesses, with its growing resistance variations complicating treatment development. Studies have emphasized the importance of virulence factors *OprE* and *OprF* in pathogenesis, highlighting their potential as vaccine candidates. In this study, B-cell, MHC-I, and MHC-II epitopes were identified, and molecular linkers were active to join these epitopes with an appropriate adjuvant to construct a vaccine. Computational tools were employed to forecast the tertiary framework, characteristics, and also to confirm the vaccine's composition. The potency was weighed through population coverage analysis and immune simulation. This project aims to create a multi-epitope vaccine to reduce *P. aeruginosa*–related illness and mortality using immunoinformatics resources. The ultimate complex has been determined to be stable, soluble, antigenic, and non-allergenic upon inspection of its physicochemical and immunological properties. Additionally, the protein exhibited acidic and hydrophilic characteristics. The Ramachandran plot, ProSA-web, ERRAT, and Verify3D were employed to ensure the final model's authenticity once the protein's three-dimensional structure had been established and refined. The vaccine model showed a significant binding score and stability when interacting with MHC receptors. Population coverage analysis indicated a global coverage rate of 83.40%, with the USA having the highest coverage rate, exceeding 90%. Moreover, the vaccine sequence underwent codon optimization before being cloned into the *Escherichia coli* plasmid vector pET-28a (+) at the EcoRI and EcoRV restriction sites. Our research has developed a vaccine against *P. aeruginosa* that has strong binding affinity and worldwide coverage, offering an acceptable way to mitigate nosocomial infections.

Keywords: *Pseudomonas aeruginosa*; *OprE* and *OprF*; immunoinformatics; multi-epitope vaccine

Introduction

Pseudomonas aeruginosa is considered to be one of the three most harmful bacteria according to the World Health Organization (WHO); therefore, research on this matter must be performed immediately with the aim of discovering novel therapies. This bacterium is a pathogen known to be resistant to many drugs, such as *Enterococcus faecium*, *Staphylococcus aureus*, *Klebsiella pneumoniae*, *Acinetobacter baumannii*, and *Enterobacter* species. They have been acknowledged as a substantial contributor to the prevalence of disease, fatalities, and economic burden on healthcare systems worldwide [1–4]. *P. aeruginosa* belongs to the common Gram-negative bacteria, which can potentially be detected in a wide range of environments. *P. aeruginosa*, a well-known pathogen, is recognized as the causative agent of various life-threatening diseases [5, 6]. Poisons that frequently arise in various healthcare environments include soft tissue and burn infections, and pneumonia associated with ventilators, in addition to chronic pulmonary infections in those who have cystic fibrosis (CF). Since *P. aeruginosa* infections are becoming more common, WHO has prioritized research and development of potential medications. [7].

The genome of *P. aeruginosa* is composed of an adaptable accessory element and an unchanging core. The bacteria may adjust to a wide range of environments corresponding to their genetic arrangement, including biofilms in ventilators and catheters as well as agricultural settings. The genetic variety of *P. aeruginosa* provides it with a diverse range of transporters, regulatory proteins, and signalling systems that improve its capacity for metabolic modification and survival [8–11]. *P. aeruginosa* uses a multifaceted style to grow inside a host, attaching itself to the host cell through cell surface components

Received: May 22, 2024. **Revised:** July 16, 2024. **Accepted:** July 30, 2024

and releasing toxic substances and effector proteins through bacterial mechanisms that help them escape or modify the host's immune system (e.g. through type III secretion systems). Bacteria use many type IV pili to adhere to cell surfaces and flagella to move throughout people with a weakened immune system. The lipopolysaccharide and exopolysaccharide alginate of *P. aeruginosa* act as crucial surface particles that support adhesion to host cells and improve the persistence of the bacterium in the host surroundings [12–14].

Many different proteins make up the outer membrane of *P. aeruginosa* and are essential for stabilizing and shielding the bacteria. Proteins show indispensable roles in the control and also the increase of molecular transport across cellular membranes. These proteins exhibit consistent preservation throughout different serogroups of *P. aeruginosa* and retain their phenotypic stability even in the presence of biofilms. The combined action of external and released constituents has been found to have a significant impact on the immune response of the host, along with the damage imposed on host tissues and the overall virulence of bacteria. As a consequence, multiple elements have been recognized by the adaptive immune system and have undergone extensive research as potential targets for the development of vaccines [14–16]. The diverse range of virulence factors exhibited by *P. aeruginosa* allows it to induce a multitude of disease manifestations, establishing its status as a significant pathogen in humans [17]. The ability of this pathogen to induce infections in various anatomical regions, such as the pulmonary and renal system, skin and soft tissues, and the eyes and ears, has been extensively studied [18, 19]. Infections of this nature primarily affect individuals who have physical barriers, reduced phagocytic functions, or weakened immune systems. The presence of *P. aeruginosa*, a pathogen frequently encountered in hospital environments, poses a considerable obstacle to healthcare. It accounts for 17% of pneumonia cases linked to the use of ventilators, 9% of other pneumonia cases acquired within hospital settings [20, 21], 10% of urinary tract infections associated with catheters, 4% of bloodstream infections originating from central lines, and 6% of infections occurring at surgical sites. In addition, *P. aeruginosa* is noteworthy for being the main source of lung infections in CF patients, which significantly increases morbidity and death rates in this population [22, 23]. It has been identified as a commonly encountered pathogen among military personnel who have returned from battlefields in Iraq and Afghanistan. These individuals often present with infections that are directly linked to war-related activities [24, 25]. Outside of the battlefield, burn wound infections are an urgent concern for these bacteria since the individuals who suffer from them are becoming less responsive to antibiotics. Furthermore, individuals receiving chemotherapy who have advanced neutropenia—a decrease in neutrophil count—are more vulnerable to *P. aeruginosa* infections, which may include serious illnesses such as bloodstream infections and pneumonia [26]. An efficient vaccination must be developed immediately since *P. aeruginosa* may cause a broad variety of diseases and is becoming more resistant to medications [27–30]. Our goal was to reduce *P. aeruginosa*–related morbidity and death by developing a multi-epitope vaccine by leveraging epitopes obtained from *OprE* and *OprF* via the use of immunoinformatics methods.

Materials and Methods

Retrieval of protein sequence

An extensive review of the subject of research was performed to determine which proteins would be best for creating a multi-epitope vaccine. *OprE* (accession id: GLF06114) and *OprF* (UniProt id: P13794) are two significant outer membrane proteins from *P. aeruginosa*. The UniProt database was consulted in order to get the FASTA formatted protein sequences for these proteins. The ExPASy ProtParam via the web was implemented to evaluate the candidate proteins' physical and chemical characteristics [31]. Moreover, the VaxiJen server version 2.0 assessed the protein's antigenicity [32]. VaxiJen has carried out an antigenicity analysis by applying the utilization of data that accumulates from the physical and chemical attributes of the protein. The sequences (*OprE* and *OprF*) were compared using the NCBI protein–protein BLAST program to reduce the likelihood of cross-reaction and the formation of autoimmune conditions against human proteins.

Immune epitope estimation

Regarding the development of vaccines, B-cell epitopes possess the greatest interest as they stimulate the humoral immune response, leading to the production of antibodies that can efficiently eliminate pathogen antigens during an illness. A threshold of 0.5 was employed in our application of the Bepipred Linear Epitope Prediction 2.0 technique, which is accessible via the web server of the Immune Epitope Database (IEDB), to generate projections about sequence-based linear B-cell epitopes for two target proteins [33, 34]. For the purpose of our inquiry, we applied the default settings and uploaded the FASTA sequences of the protein. After identifying these B-cell epitopes, we evaluated their ability to serve as MHC-I and MHC-II epitopes using the MHC-I and MHC-II binding prediction tool on the IEDB website, using human HLAs as the benchmark. With all reference sets of human HLA alleles, MHC-I epitopes were discovered utilizing the 2020.09 approach (NetMHCpan EL 4.1) as specified by the IEDB. The IEDB analytical resource MHC-II binding tool, which covers HLA alleles like human HLA-DR, was employed to undertake MHC-II binding projections. The corresponding binding alleles were determined utilizing the NetMHCIIpan EL 4.1 technique, with human HLAs serving as the standard reference set (see Supplementary Table S1 available online at http://bib.oxfordjournals.org/) [35]. The epitopes that were chosen had elevated antigenicity scores (see Supplementary Tables S2 and S3 available online at http://bib.oxfordjournals.org/). In addition, these epitopes were examined for their allergic, poisonous, and soluble properties as described in the next section [36–39].

Epitope characterization

The antigenic properties of the reported epitopes were verified utilizing the VaxiJen v2.0 program, resulting in a suitable limit of 0.4. The *k*-nearest neighbours' method (kNN, $k = 1$) and the autocross covariance (ACC) for sequence conversion were employed for arranging epitopes in the AllerTOP v2.0 system, which was utilized to test the peptides' allergenicity potential (https://www.ddg-pharmfac.net/AllerTOP/). ACC is a technique that converts protein sequences into vectors whose length can be accurately estimated. The kNN method ($k = 1$) was employed with a training set of 2427 known allergens and 2427 non-allergens from distinct species [40]. The toxicity of the targets was studied using the default configuration of the ToxinPred server, which incorporates an Support Vector Machine (SVM) (Swiss-Prot-)-based algorithm [41]. In addition, the solubility of these epitopes was assessed using the default settings of the Innovagen Peptide Calculator (https://pepcalc.com/).

Vaccine construction

Through the application of suitable linkers, including EAAAK and GPGPG, the adjuvant cholera toxin B, as well as certain B-cell, MHC-I, and MHC-II epitopes, was combined to produce the

vaccine. The prospective vaccine candidates, the epitopes, were connected by GPGPG linkers [42]. The adjuvant, which is typically employed to boost the effectiveness of vaccine, was coupled to the epitopes employing the EAAAK linker [43]. A substantial improvement in the comprehensive immunogenicity of the multi-epitope peptide may be achieved with the incorporation of an adjuvant substance [44]. As a result of the fact that they favour epitope exhibition to the immune system and permit for effective immunological release, GPGPG linkers were used in the construction of the epitope peptide combination [45]. These linkers ensure that the protein is as flexible as possible while also facilitating the accurate folding of amino acids into the proper conformations.

Characteristics and molecular conformations of the vaccine

We investigated the vaccine's chemical and biological characteristics employing the ExPASy ProtParam database. This program availed application to protein sequence data to estimate several properties, such as molecular weight, solubility, theoretical isoelectric point (*pI*), *in vitro* half-life, and GRAVY (grand average of hydropathy). The secondary structure was anticipated to employ two website servers: SOPMA and PSIPRED.

Structure prediction and justification

We applied I-TASSER (Iterative Threading Assembly Refinement) to generate the three-dimensional structure. The structure obtained from the experiment was subjected to additional refinement using the GalaxyRefine2 service. Through the utilization of PROCHECK to produce a Ramachandran plot, which can be available at https://servicesn.mbi.ucla.edu/PROCHECK/, the validity of the model was evaluated. The server assesses the model's geometry and forecasts its stereochemical quality employing a set of programs named PROCHECK. The energetically viable torsional angles of a peptide's residues, phi (υ) and psi (ψ), are illustrated graphically by a Ramachandran plot. The model's dependability has been demonstrated by the percentages of residues in the allowed and disallowed areas. The projected tertiary structure's accuracy was further analysed through the ProSA-web platform. The Z-score is calculated by this site; a number greater than zero indicates that the protein model may include flaws or instability. Moreover, model quality was determined employing Ramachandran diagrams (https://saves.mbi.ucla.edu/), which show the acceptable zones for amino acid conformations inside a protein structure.

Population coverage screening

The Population Coverage tool (IEDB) was employed for assessment how racial, regional, and national variations in epitope affinity for HLA alleles affect the creation of epitope-based vaccines. For this investigation, 23 geographical locations were selected using the default parameters. This study analysed the human MHC binding allele distribution to measure the scope of population coverage of T-cell epitopes across various geographical regions [46].

Discontinuous B-cell epitope assessment

The ElliPro server was employed to estimate discontinuous B-cell epitopes. The server operated successfully with an initial residue number of 0.5 and an optimal distance of 6 Å when configured as default. The Protrusion Index (PI) allocates a sign to every epitope that produces the average of all the PI values for every residue inside the epitope. This approach correlates the three-dimensional protein structure by ellipsoids. With a PI score of 0.9, it is assumed that 90% of the protein's residues are located within the ellipsoid and 10% are outside of it. The centre of mass of each residue is utilized to figure out the PI number and show if the residue fits inside the ellipse. The PI values of discontinuous epitopes help find them, and the distance parameter *R*, which contributes to how close the centres of mass of residues are to each other, decides how they are grouped. A higher *R* number means that there are more likely to be multiple discontinuous epitopes.

Docking and molecular dynamics simulation

Cluspro 2.0 employs rigid-body docking to predict protein interactions. This software is extremely automated and efficient. It uses three primary processes grouping the best energy conformations, using a particular correlation based on fast Fourier transform, and executing brief Monte Carlo simulations to assess cluster stability. The MHC-I (PDB ID: 5xs3) and MHC-II (PDB ID: 3l6f) proteins, which were extracted from the RCSB's PDB database, were customized for docking analysis with PyMol software. The best conformations were then shown for protein–protein interactions using PyMol. The docked complex's stability and physical properties were monitored via the iMODS web server (http://imods.Chaconlab.org). This platform predicts protein-coordinated movements employing internal dihedral coordinates using normal mode analysis (NMA). The iMODS analysis assessed the vaccine–receptor complex's deformability, B factor, eigenvalues, variance, covariance map, and elastic network. These analyses revealed an essential understanding of the complex's structural movements.

Immune simulation

Actual vaccine immunogenicity was assessed employing the C-ImmSim server. Machine learning and the PSS matrix produce immunological and peptide interaction assumptions in the agent-based C-ImmSim dynamics simulator. The time span between the first and subsequent administrations of vaccination was a minimum of 4 weeks. As a result, 3 doses of 1000 vaccine proteins were given at intervals of 4 weeks at time points 1, 84, and 168 (with the time point representing 8 h, with time point 1 corresponding to the first injection at time = 0). As a consequence, there were cumulatively 1050 simulation steps. The settings of the C-ImmSim immune simulator were modified appropriately, but all other parameters remained at their default levels. To investigate clonal selection and simulate recurrent exposure to an antigen in a normal milieu where the antigen is prevalent, three injections of the chosen peptide were administered at 4-week intervals. The Simpson index (*D*), which quantifies diversity, was computed based on the obtained data.

Codon optimization and cloning

We employed *in silico* cloning approaches to gain a better knowledge of the expression patterns of our newly generated vaccine candidate in hosts of *Escherichia coli*. Operating the Java Codon Adaptation Tool (JCAT) website, the vaccine was enhanced and expression was achieved in the *E. coli* K12 strain. The study's findings frequently suggest that the codon adaptation index (CAI), which is calculated by the JCAT's output, should be >0.8 and closer to 1.0. This indicates that the nucleotide sequence consists of the codons that occur the most often [47]. Furthermore, the GC content percentage must be within the designated range of 30% and 70% [48, 49]; in prokaryotes, greater GC concentration corresponds with improved protein expression [50]. The locations that were circumvented included the bacterial ribosome binding site, the Rho-independent transcription termination site, and

Table 1. Porin *OprE* and *Porin F* protein models for B-cell epitopes and immunogenicity

Protein	Epitope sequence	Start position	Antigenicity score	Allergenicity	Toxicity	Solubility
Porin *OprE*	KGDNIKSGRGDQSEW	391	1.8879	Non-allergen	Nontoxic	Good water solubility
	GLPVSGSGTATQRDQ	435	1.5728			
Outer membrane porin F	DKSKVKE	247	1.2018			
	YGESRPVADNATAEGRA	320	0.9562			

the restriction enzyme cleavage site. The vaccine's optimized nucleotide sequence was cloned into the *E. coli* pET-28a (+) vector using Snap Gene 5.2.4. In the N- and C-terminal edges of the sequence, EcoRI and EcoRV restriction sites were accordingly inserted.

Results

Retrieval of protein sequence

OprE (accession ID: GLF06114) and *OprF* (UniProt ID: P13794) are two important outer membrane proteins from *P. aeruginosa*. The UniProt database produced protein sequences in FASTA format, which were then examined for antigenic potential using the VaxiJen v2.0 server. The investigation produced antigenic values higher than the cutoff point of 0.4, with OprE yielding 0.8657 and OprF yielding 0.8044. The ExPASy ProtParam web server was employed to further examine the physical and chemical properties of these proteins (see Supplementary Tables S4 and S5).

Projection of linear B-cell epitopes

The expression of antigen-specific antibodies in serum was increased by B-cell epitopes. When immunogenic epitopes attach to B-cell receptors in the natural world, the generation of antibodies begins, and the cells differentiate into memory and plasma cells. Memory cells contribute to the generation of secondary infection antibodies, while plasma cells are in charge of producing primary antibodies during the original infection. Therefore, the development of epitope-based vaccine depends on discovering B-cell epitopes within marker proteins. The epitopes that scored higher than the cutoff of 0.5 were selected. Among the 26 expected epitopes (see Supplementary Table S6), four (KGDNIKSGRGDQSEW, GLPVSGSGTATQRDQ from porin *OprE*, and DKSKVKE, YGESRPVADNATAEGRA from porin F) fulfilled the criteria defined above and were chosen for vaccine development (Table 1).

Projection of MHC binding epitopes

HTL-activating epitopes were discovered by using the IEDB service to find peptides that engage with MHC-I and MHC-II molecules. Targeting 54 predominant human alleles, the NetMHCpan EL 4.1 method was implemented to forecast MHC-I epitopes. Using the NetMHCIIpan EL 4.1 approach, 27 alleles were selected for MHC-II epitopes (see Supplementary Tables S2 and S3 available online at http://bib.oxfordjournals.org/). The epitopes' allergenicity, toxicity, solubility, and antigenicity were additionally assessed. The scores of the top three putative epitope candidates associated with distinct MHC class alleles are presented in Tables 2 and 3.

Vaccine construction

The final vaccine formulation contained cholera toxin B as the adjuvant, which was connected to the B-cell epitope at the N-terminal end by an EAAAK linker. Two B-cell epitopes were separated by GPGPG linkers, and then MHC-II peptides were inserted to join them. Lastly, the MHC-I epitopes were attached at the C-terminal end employing a GPGPG linker. Figure 1A presents the vaccine graphically.

Physicochemical and secondary structure of vaccine

Physicochemical characteristics of the designed vaccine revealed an estimated isoelectric point (p*I*) of 9.17 and a molecular weight of 40 764.71 kDa. It was estimated to have an *in vitro* half-life of 30 h in mammalian reticulocytes and an *in vivo* half-life of >20 h in yeast and 10 h in *E. coli*. The vaccine was determined to remain stable, as evidenced by an instability index score of 23.63 (values exceeding 40 points to instability). The vaccine's thermostability was indicated by an aliphatic index of 47.27, while its hydrophilic nature was demonstrated by a GRAVY score of −0.827. The protein has a high solubility following expression, as demonstrated by its calculated solubility score of 0.586. According to the SOPMA technique, 21.87% of the isolates were alpha helices, 11.55% were extended strands, 6.14% were beta twists, and 60.44% were random coils (Fig. 1B).

Vaccine 3D structure: prediction, refinement, and validation

A 3D configuration was generated using the I-TASSER server. From 10 threading templates, 5 3D structural models were predicted with *Z*-scores ranging from 0.67 to 1.01 and *C*-scores ranging from −5 to −4. The model's confidence is indicated by its *C*-score, which ranges from −0.5 to 2. The model chosen for further examination has the highest *C*-score of −0.67. The model according to evaluation had a root-mean-square deviation of 8.4 ± 4.5 Å and a Template Modeling (TM) value of 0.63 ± 0.14, as shown in the information provided in Fig. 2A. The TM score was calculated to evaluate the models' structural similarity.

Five unique vaccine variants were produced from the initial version. Model 5 proved to be the most significant model according to structural parameters such as the Rama value (89.4), weak rotamers (0.0), GDT-HA (0.8888), RMSD (0.835), and MolProbity (1.887). For more research, this model was selected (Fig. 2B). The Ramachandran plot analysis was employed to confirm the structure of the vaccine. The results showed that 79.7% of the residues were in the most favoured regions, 18.4% were in the allowed regions, and 1.8% were in the prohibited regions (Fig. 2C). In addition, the ERRAT analysis determined that the updated model had an overall quality factor of 81.152%, as shown in Fig. 2D. The *Z*-score of the model, calculated using the ProSA, was found to be −4.85 (Fig. 2E). Overall, the results from computational applications of RAMPAGE, ERRAT, and ProSA-Web demonstrated the tertiary structure quality of the vaccine.

Population coverage investigation

T-Cell epitopes that bind to several HLA super types alleles were sought for wide population coverage. The MHC-I and MHC-II (T-cell) epitope-specific IEDB database tool was utilized to estimate

Table 2. Potential MHC-II epitopes from porin *OprE* and *Porin F* proteins and their immunogenicity

Protein	Epitope sequence	Allele	Antigenicity score	Allergenicity	Toxicity	Solubility
Porin *OprE*	GTVDGGGRAGKSGLG	HLA-DQA1*05:01	2.4582	Non-allergen	Nontoxic	Good water solubility
	TQGTVDGGGRAGKSG	HLA-DQA1*05:01	2.4616			
	TVDGGGRAGKSGLGL	HLA-DQA1*05:01	2.3598			
Outer membrane porin F	DAYNQKLSERGVEGY	HLA-DRB1*08:02,HLA-DQA1*04:01,HLA-DRB1*11:01	1.6339			
	NINSDSQGRQQMTTE	HLA-DRB1*03:01	1.8418			
	TDAYNQKLSERGVEG	HLA-DRB1*08:02,HLA-DQA1*04:01,HLA-DRB1*11:01	1.8237			

Table 3. Reported MHC-I epitopes from porin *OprE* and *Porin F* proteins and their immunogenicity

Protein	Epitope sequence	Allele	Antigenicity score	Allergenicity	Toxicity	Solubility
Porin *OprE*	DGKNGSRSGR	HLA-A*33:01	3.2546	Non-allergen	Nontoxic	Good water solubility
	SGSGTATQR	HLA-A*31:01,HLA-A*68:01	2.9601			
	TVDGGGRAGK	HLA-A*11:01	2.7645			
Outer membrane porin F	DAYNQKLSER	HLA-A*68:01,HLA-A*33:01	1.7436			
	KLSERGVEGY	HLA-B*15:01,HLA-A*30:02,HLA-A*01:01,HLA-A*03:01	1.7199			
	NSDSQGRQQM	HLA-A*01:01	2.141			

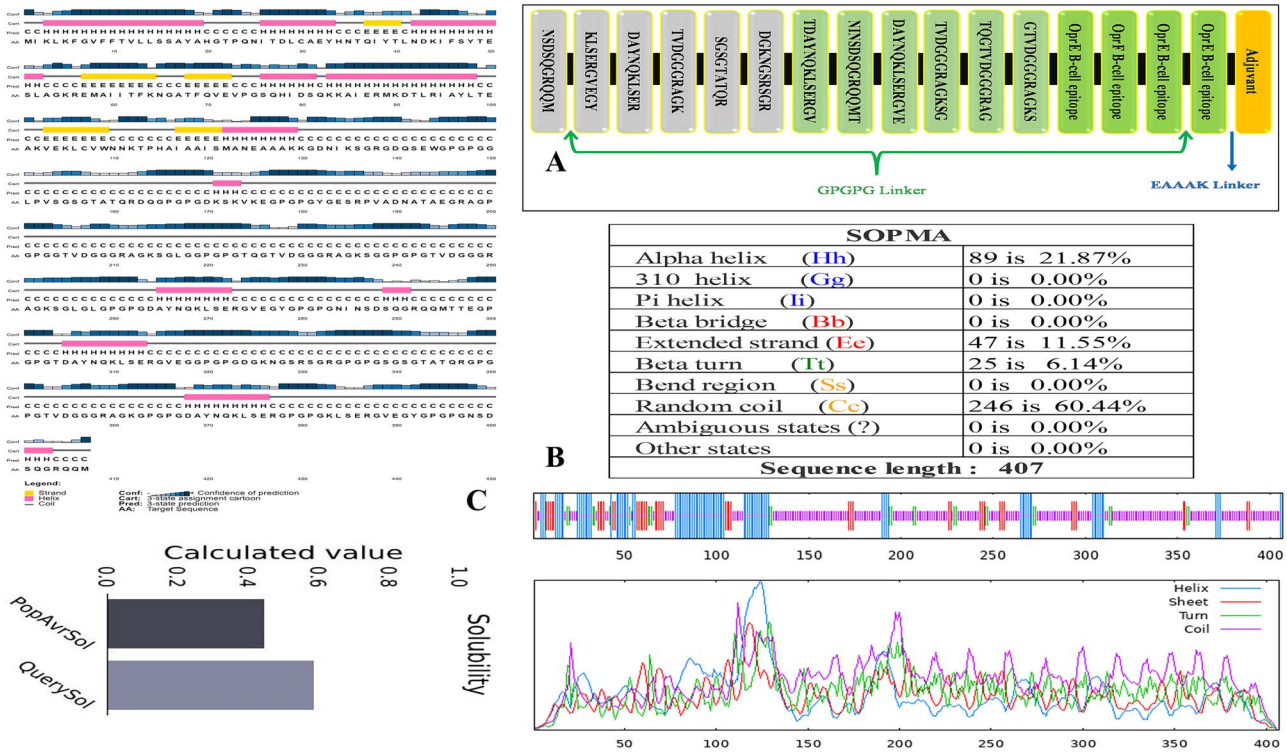

Figure 1. (A) The multi-epitope vaccine possesses 407 amino acids. The N-terminal EAAAK linker includes the cholera toxin B buffer peptide. GPGPG linkers coupled B-cell, MHC-II, and MHC-I epitopes. (B) SOPMA secondary structure analysis revealed 21.87% alpha helices, 11.55% extended strands, 6.14% beta twists, and 60.44% random coils in the vaccine. (C) PSIPRED predicts vaccine construct solubility and secondary structure.

the geographic coverage of these anticipated epitopes. This analysis encompassed 16 geographical regions across 6 significant countries. According to population coverage analysis, 83.40% of the population would be safeguarded by the proposed vaccine worldwide. Notably, the predicted epitope core sequences demonstrated substantial variations in population coverage rates. As illustrated in Fig. 3, the territories of the USA and Japan exhibited the highest and lowest coverage rates, respectively.

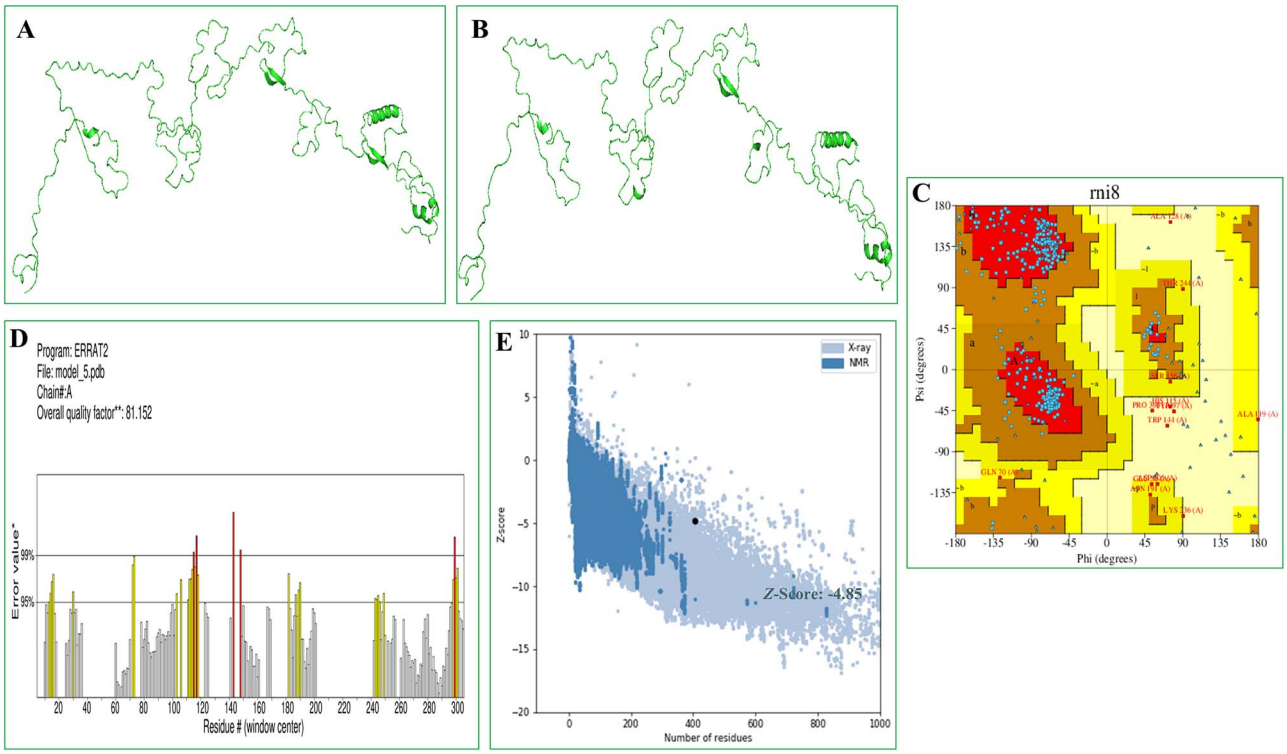

Figure 2. Vaccine 3D structure prediction, refinement, and validation. (A) The initial 3D structure of the vaccine (I-TASSER). (B) GalaxyRefine aided in refining the three-dimensional structure. (C) The residues in the Ramachandran plot were classified as 79.7% favourable, 18.4% acceptable, and 1.8% in the disallowed zone. (D) With an ERRAT quality aspect of 81.152%. (E) According to the ProSA-web evaluation, the E.Z. was −4.85.

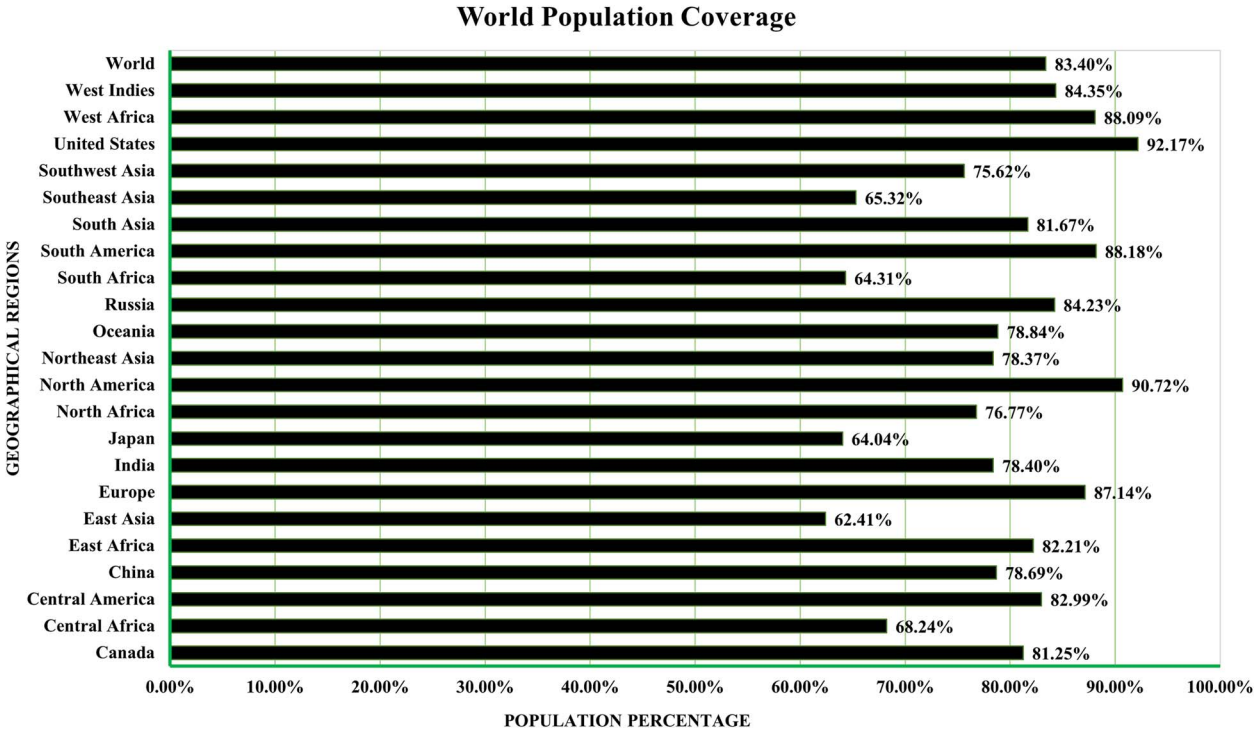

Figure 3. HLA allele population coverage for particular epitopes by area and nation.

Discontinuous B-cell epitopes

A total of 212 residues were found in 13 discontinuous B-cell epitopes, corresponding to the ElliPro server information. The epitopes' lengths encompassed >3 to 37 residues, while their scores varied from 0.502 to 0.971. The peptides that were discontinuous are demonstrated in Fig. 4 (1–14).

Docking and molecular dynamics simulation

The ClusPro 2.0 server was employed to carry out protein–protein interaction between the vaccine and human immunological receptors. The model that exhibited the lowest energy value was deemed the most optimally docked of the 30 representations produced by the server. The results, shown in Fig. 5A and B,

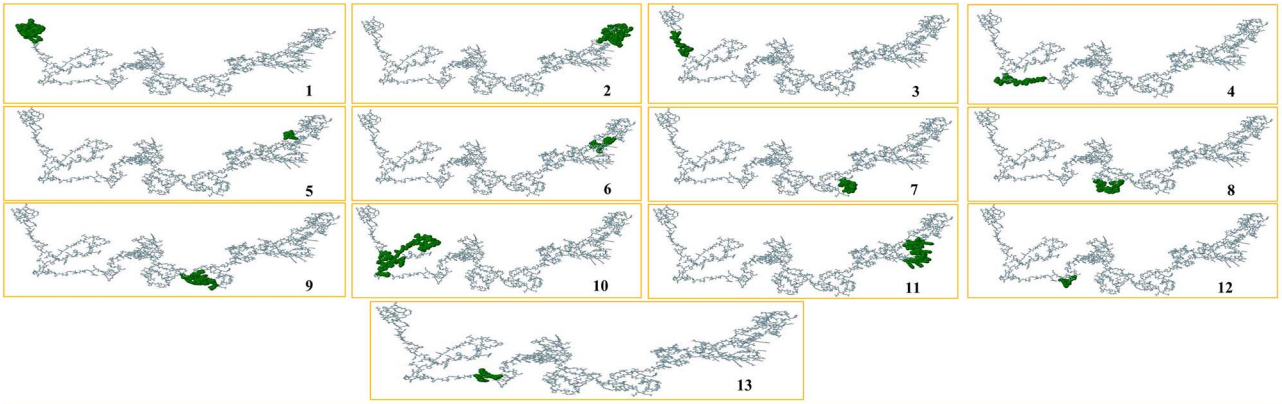

No.	Residues	Number of residues	Score
1	A:R387, A:G388, A:V389, A:E390, A:G391, A:Y392, A:G393, A:P394, A:G395, A:P396, A:G397, A:N398, A:S399, A:D400, A:S401, A:Q402, A:G403, A:R404, A:Q405, A:Q406, A:M407	21	0.971
2	A:K3, A:L4, A:K5, A:F6, A:G7, A:V8, A:F9, A:F10, A:T11, A:V12, A:L13, A:L14, A:S15, A:S16, A:A17, A:Y18, A:A19, A:H20, A:G21, A:T22, A:P23, A:Q24, A:N25, A:I26, A:T27, A:D28, A:L29, A:C30, A:A31, A:E32, A:Y33, A:H34, A:N35, A:T36, A:Q37, A:I38, A:Y39	37	0.883
3	A:R377, A:G378, A:P379, A:G380, A:P381, A:G382, A:K383, A:L384, A:S385, A:E386	10	0.823
4	A:G315, A:V316, A:E317, A:G318, A:G319, A:P320, A:G321, A:P322, A:G323, A:D324, A:G325, A:K326, A:N327, A:G328, A:S329	15	0.764
5	A:T40, A:L41, A:N42	3	0.74
6	A:D43, A:K44, A:I45, A:F46, A:S47, A:Y48, A:T49, A:E50, A:S51, A:L52, A:A53, A:G54, A:K55	13	0.692
7	A:D163, A:Q164, A:G165, A:P166, A:G167, A:P168, A:G169, A:D170, A:K171, A:S172, A:K173	11	0.662
8	A:G210, A:A212, A:G213, A:K214, A:S215, A:G216, A:L217, A:G218, A:G219, A:P220, A:G221, A:P222, A:G223, A:T224, A:Q225, A:G226	16	0.657
9	A:V153, A:S154, A:E176, A:G177, A:P178, A:G179, A:P180, A:G181, A:Y182, A:G183, A:E184, A:S185, A:R186, A:P187, A:V188, A:A189, A:D190, A:N191, A:A192, A:T193	20	0.656
10	A:R330, A:S331, A:G332, A:R333, A:G334, A:P335, A:G336, A:P337, A:G338, A:S339, A:G340, A:S341, A:G342, A:T343, A:A344, A:T345, A:Q346, A:R347, A:G348, A:P349, A:G350, A:P351, A:G352, A:T353, A:V354, A:D355, A:G356, A:A369, A:Y370, A:N371, A:Q372, A:K373, A:L374, A:S375, A:E376	35	0.605
11	A:R56, A:E57, A:M58, A:A59, A:I60, A:F69, A:Q70, A:V71, A:E72, A:V73, A:P74, A:G75, A:S76, A:Q77, A:H78, A:I79, A:D80, A:S81, A:Q82, A:K83, A:K84, A:A85, A:E87, A:R88	24	0.559
12	A:A306, A:N308, A:K310	3	0.55
13	A:L311, A:S312, A:E313, A:R314	4	0.502

Figure 4. The ElliPro server predicts discontinuous B-cell epitopes for multi-epitope vaccination. 1–13. The green surface has discontinuous B-cell epitopes. 14. Discontinuous B-cell epitope residues and score.

demonstrated that the vaccine exhibits significant binding affinity to both MHC-I and MHC-II receptors, the corresponding binding strengths of 865.4 kcal/mol and 879.6 kcal/mol, respectively. The outcomes of this investigation demonstrated that the vaccine may interact with immune receptors in an efficient manner and stimulate substantial immune responses (Fig. 5).

The iMOD server was employed to conduct NMA to assess the vaccine's stability in combination with MHC-I and MHC-II. A significant level of deformability was observed in the regions featuring hinges, as illustrated in Figs. 6 and 7. The B-factor values revealed a direct relationship with the root mean square in the normal mode analysis. Specifically, the eigenvalues for the MHC-I complex were determined to be 2.534410×10^{8}, and those for the MHC-II complex were 2.869817×10^{8}. The energy necessary for structural deformation is denoted by these values; value reduction indicates easier deformation. The relationships between residue pairs are depicted in the covariance matrix, whereas the interatomic connectivity via springs is illustrated in the elastic network model. The data suggest that the vaccine exhibits prolonged interactions with MHC-I and MHC-II.

Immune simulation

The results obtained from immune simulations completed by the C-ImmSim server exhibited a notable enhancement in immune responses that displayed similarities to genuine immunological reactions. An elevation of the IgM concentration revealed the most significant response. The antigen levels decreased while the B-cell population, IgG1 + IgG2 antibodies, and IgG + IgM antibodies increased in response to secondary and tertiary injections. In addition, memory cells and TC cells could be incorporated into a vaccine model to augment the TH population. Additionally, IFN- and IL-2 production increased with repeated exposure. These findings confirmed the vaccination model's immunogenic and antigenic characteristics (Fig. 8).

Codon optimization and *in silico* cloning

A specific amino acid being programmed by multiple codons in distinct organisms results in codon bias. Identical amino acids may be transcribed using distinct codons due to variations in the cellular machinery between organisms. Predicting the most efficient codon for encoding a specific amino acid in a given organism was the objective of this investigation, which applied codon adaptation. The microorganism *E. coli* strain K12's codon was optimized using the java codon adaptation tool. Restriction enzyme cleavage sites, including EaeI and StyI, rho-independent transcription terminators, and bacterial ribosome binding sites, have been reported to the server. The optimized sequence showed a CAI of 0.966 and a GC content of 55.937%, in contrast to the native GC level of *E. coli*, which was 50.734%. Afterwards, locations for restriction enzymes were searched for in the codon-optimized vaccine construct sequence; EcoRI and EcoRV enzymes were not identified in the vaccine. In order to facilitate *in silico* cloning, these enzymes were consequently encompassed into vaccine candidates. Eventually, a successful clone of 5205 bp was generated after placing the vaccine into the pET28a (+) vector, as shown in Fig. 9.

Discussion

The major membrane proteins of *Pseudomonas* play diverse roles during visceral infections, aiding bacterial growth in high-osmolarity environments, impeding macrophage microbicidal functions, and influencing susceptibility to antimicrobial peptides [51]. To develop more effective immunization strategies against *P. aeruginosa*, it is essential to identify the immunogenic

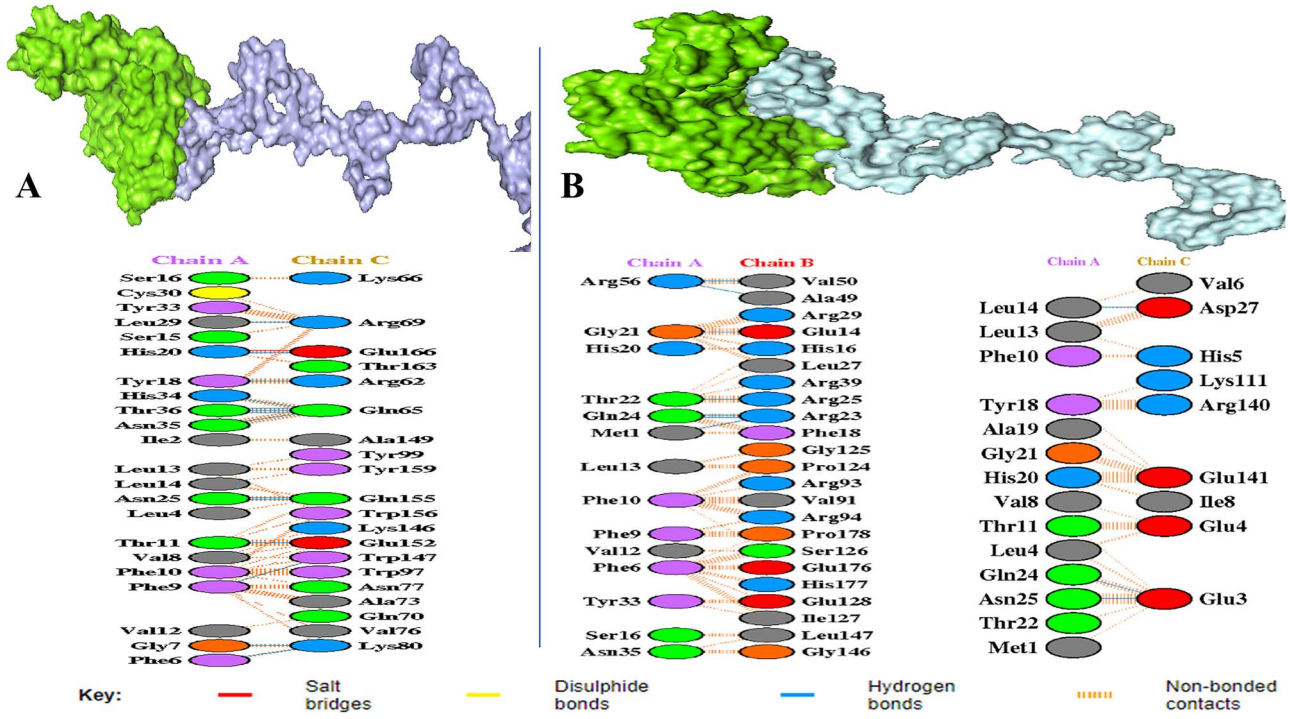

Figure 5. (A) MHC-I receptor with a vaccine candidate interaction between chain A and chain B. (B) MHC-II receptor with vaccine candidate interaction between chain A and chain B and chain C. The interaction analysis was predicted by the web server (PDBsum) and virtualized by PyMOL.

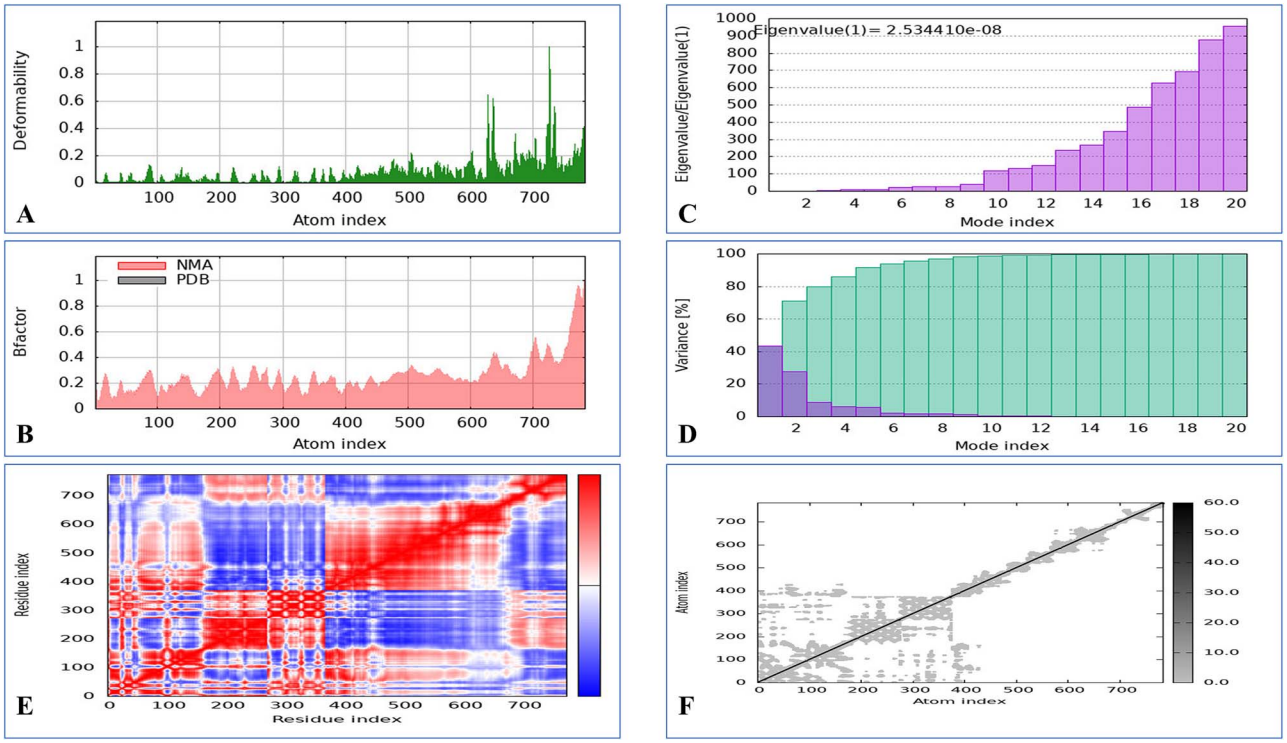

Figure 6. Molecular dynamics simulation of a vaccine model with MHC-I includes several aspects. (A) Analysis of deformability through molecular dynamics simulations. (B) Examination of B-factors. (C) Evaluation of eigenvalues, where lower numbers indicate more facile deformation. (D) Analysis of variance, with red indicating individual variations and green indicating aggregate variances. (E) Covariance mapping, with red representing correlated regions, white demonstrating no correlation, and blue representing anti-correlation. (F) Elastic network analysis, where darker areas suggest increased stiffness.

epitopes of the essential membrane-associated proteins of *P. aeruginosa*, such as *OprE* and *OprF*, as well as their interactions with the MHC alleles of the host and immune cells. A technique that recently appeared to be an economical, quick, and dependable method for detecting antigenic regions of proteins is the application of immunoinformatics methods. These methods involve an assortment of bioinformatics tools and databases. For the purpose of improving subunit vaccines,

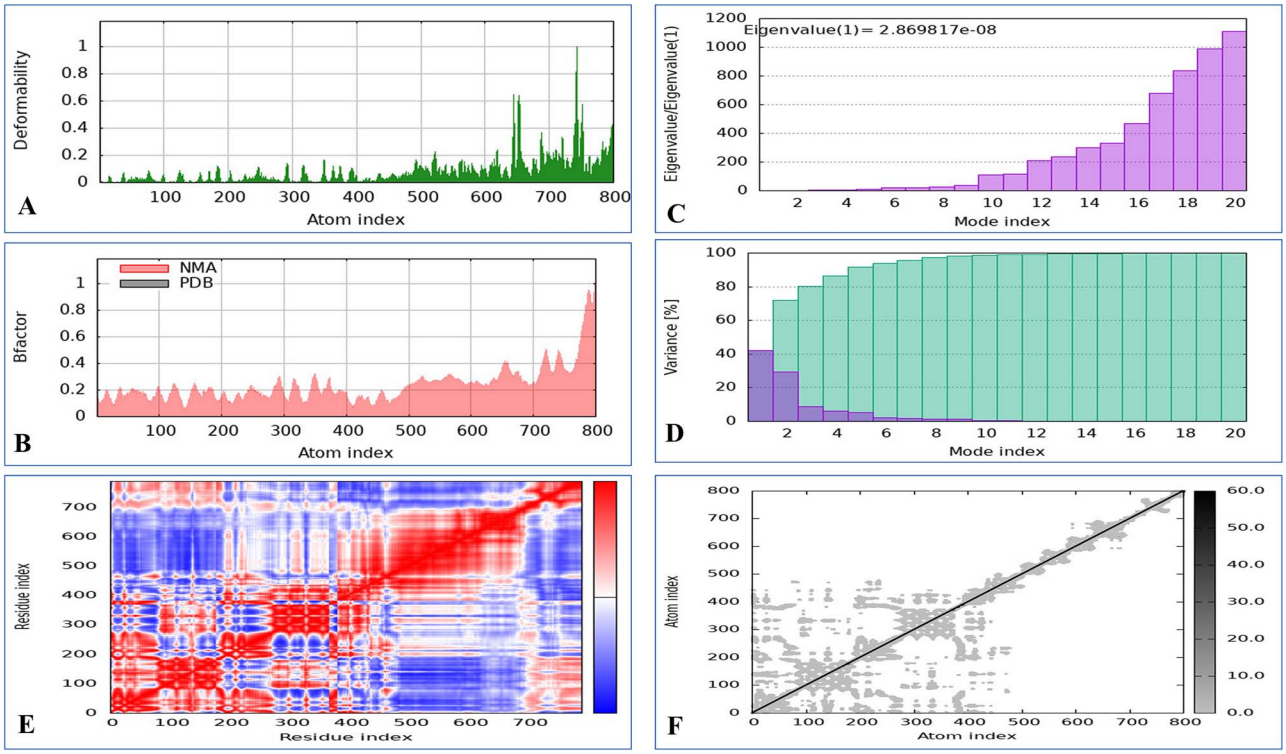

Figure 7. Molecular dynamics simulation of a vaccine model with MHC-II includes several aspects. (A) Analysis of deformability through molecular dynamics simulations. (B) Examination of B-factors. (C) Evaluation of eigenvalues, where lower numbers indicate more facile deformation. (D) Analysis of variance, with red indicating individual variations and green indicating aggregate variances. (E) Covariance mapping, with red representing correlated regions, white demonstrating no correlation, and blue representing anti-correlation. (F) Elastic network analysis, where darker areas suggest increased stiffness.

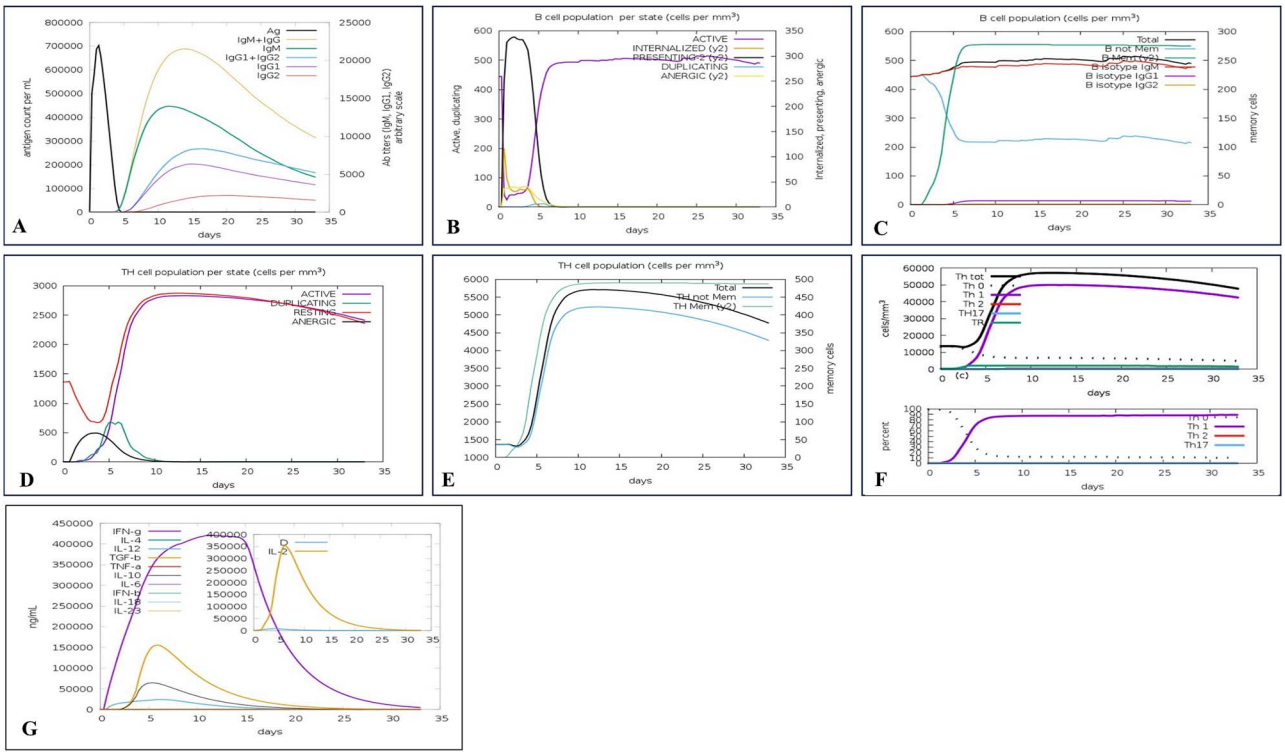

Figure 8. *In silico* immune system simulations using the C-ImmSim service include the following observations: (A) Increases in IgM and IgG responses (depicted as a cream peak) and a reduction in antigen levels (black peak) were noted after the second and third injections. (B) Activation of the B-cell population is shown by a purple peak. (C) Boosting of B cells for memory functions is indicated by a green peak. (D) TH cell activation is represented by a purple peak. (E) The enhancement of memory TH cells is shown as a green peak. (F) The T-cell response showing Th1 polarization is depicted with a purple peak. (G) Increases in IL-2 (cream peak) and IFN-γ (purple peak) in response to the vaccine.

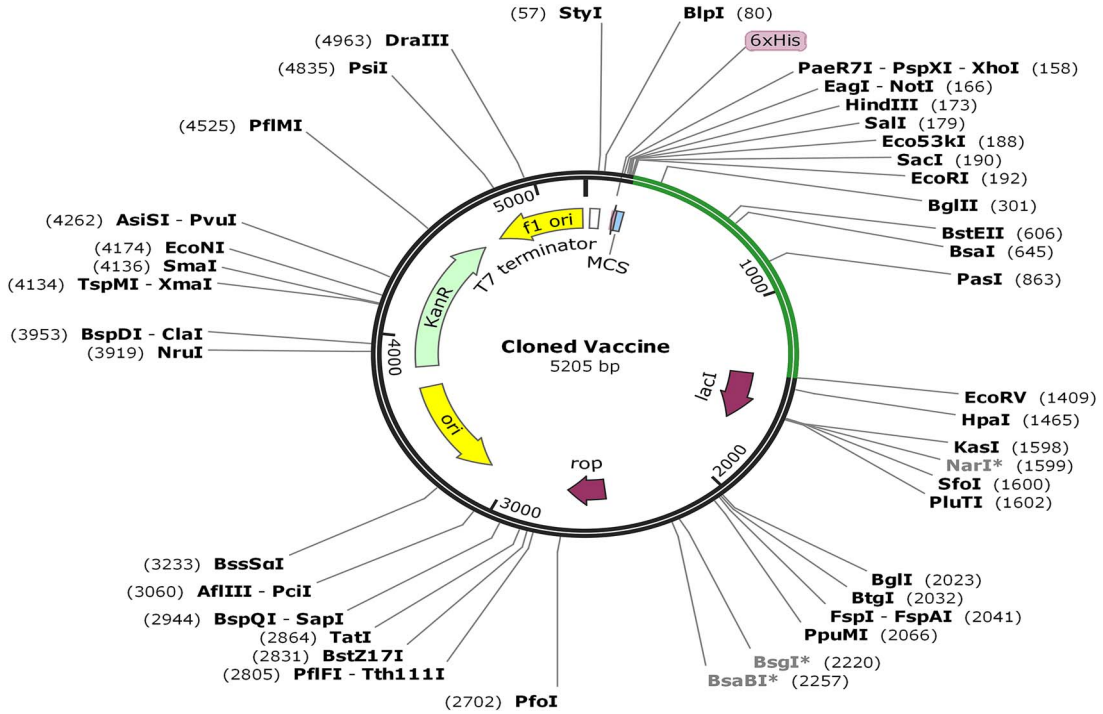

Figure 9. *In silico* pET-28a (+) vaccine cloning. The vector DNA was black, whereas the vaccination DNA was green. The SnapGene restriction sites EcoRI and EcoRV were cloned.

this method provides simpler methods for discovering promising antigens [52–55].

Therefore, the objective of this investigation was to develop an innovative multi-epitope vaccine against *P. aeruginosa* infection. The vaccine was designed through an immunoinformatics technique and focused on the main membrane proteins of the bacterium, *OprE* and *OprF* [51]. The promiscuous, highly immunogenic, nontoxic, and non-allergenic B- and T-cell (MHC-I and MHC-II) epitopes were identified by integrating the predictions generated by numerous distinct epitope prediction mechanisms. Furthermore, these epitopes exhibited a strong propensity for binding to an inclusive variety of human leukocyte antigen alleles. This was a significant finding. As a consequence, the anticipated epitopes, in conjunction with the linkers that had been constructed, were used in the process of constructing a possible vaccine, which incorporated cholera B toxin as an adjuvant [56, 57].

We noticed that our possible vaccine had a molecular weight of 40.76 kDa when we were in the midst of assessing its physicochemical properties. Considering the standard recommendation for proteins to have a molecular weight of ≤100 kDa, this quantity is within the permissible range for straightforward synthesis and purification [58]. The theoretical isoelectric point (pI) of the vaccine was 9.17, indicating an alkaline nature. Particularly noteworthy is that the vaccine had prolonged half-lives, which exceeded 10 h in *E. coli* and >20 h in yeast cells, indicating that it was visible to the immune system for an extended period of time. In standard applications, the vaccine had an elevated degree of stability, as shown by its stability index, which was <40. Furthermore, the high aliphatic index showed that the substance had outstanding thermostability, and the low GRAVY value indicated that it has hydrophilic properties [59, 60].

The secondary structural analysis revealed that the vaccine was largely composed of random coils, which represented 60.44% of the total, followed by alpha helices, which accounted for 21.87%, and extended strands (10.55%). A stable structure that was primarily characterized by random coils, which helps in identification by components of the immune system, was proposed based on these results [61]. Next, the tertiary structure of the peptides was determined by employing the I-TASSER. Afterwards, the GalaxyRefine server was employed with the goal of refining and improving the structural irregularities that emerged [62]. The examination of the projected three-dimensional model using well-established methods revealed that 79.7% of the residues were located in the chosen location. This finding is indicative of the stability and excellent quality characteristics of the proposed structural model [63].

According to an investigation that examined population coverage, the vaccine managed to safeguard 83.40% of the global population. The USA had the highest coverage percentage, which was >90% [64, 65]. Furthermore, the vaccine was docked with both MHC-I and MHC-II receptors to determine whether it could provoke an effective immunological response. According to the data, the vaccine showed the greatest binding affinity for both MHC-I and MHC-II complexes. Strong binding indicates that the vaccine peptides are likely to be effective, facilitating the activation and growth of these T cells via MHC-I molecules, which are mainly responsible for presenting endogenous antigens to $CD8^+$ cytotoxic T cells. This activation plays a crucial role in managing and resolving infections since it is necessary for locating and destroying contaminated cells. Likewise, the high binding affinity of the vaccine for MHC-II molecules, which expose $CD4^+$ helper T cells to external antigens, suggests that these cells are capable of efficiently identifying vaccine peptides. The coordination of the immune response as a whole, which includes stimulating $CD8^+$ T cells and activating B cells to produce antibodies, depends on this relationship. The vaccine candidate may be able to elicit a strong and all-encompassing immunological

response, as shown by its dual high binding affinities to MHC-I and MHC-II [66–68]. In vaccine development, verifying the stability of vaccine–receptor interactions is critical for guaranteeing successful immune responses. Following docking studies, molecular dynamics simulations demonstrated considerable stability of vaccination complexes with both MHC-I and MHC-II receptors, as evidenced by the values of 2.534410×10^8 for the MHC-I complex and 2.869817×10^8 for the MHC-II complex [56, 69, 70]. These numbers represent the energy needed for structural deformation, with lower values indicating easier deformation. This stability is required for extended antigen presentation, which promotes T-cell activation. Stable MHC-I complexes guarantee successful presentation to $CD8^+$ cytotoxic T cells, which is crucial for targeting infected cells, while stable MHC-II complexes allow for effective engagement with $CD4^+$ helper T cells, which is required for B-cell activation and immune response coordination. Thus, the substantial binding affinities and stability suggested by these simulations highlight the vaccine candidate's capacity to elicit a complete and prolonged immune response, making it a suitable option for further development [66, 71–73]. The immunological simulation results suggest that using this multi-epitope vaccine protein could generate a significant quantity of antibacterial cytokines. Additionally, it may also stimulate both humoral and innate immune responses, making it a potential option for combating *Pseudomonas* infection [47, 74]. The technique of *in silico* cloning was employed to evaluate the observation of the peptides in the *E. coli*, which served as the host organism [75, 76]. Overall, these results indicate that the recommended vaccine design is a suitable option for further research since it may be extremely stable and has potential for mass manufacturing. Further research via *in vitro* or *in vivo* tests will be necessary to clearly confirm the immunogenicity, efficacy, stability, safety, and various biophysical features of the prospective vaccine.

Conclusion

A multi-epitope vaccine targeting *P. aeruginosa* was successfully created using an immunoinformatics technique that included *OprE* and *OprF* epitopes. The vaccine displayed promising binding affinity and durability for MHC-I and MHC-II receptors, as well as widespread worldwide coverage. Codon optimization made it possible to clone the gene into a plasmid vector. This opens the door for future clinical and experimental validation, providing a viable way to treat *P. aeruginosa* infections and reduce the associated death and morbidity.

Key Points

- High affinity binding: The selected epitopes demonstrate strong and stable binding affinities for both MHC class I and class II receptors, indicating robust potential to elicit an immune response.
- Global coverage: The vaccine is designed to be effective across diverse genetic populations, ensuring broad applicability and effectiveness worldwide.
- Codon optimization and cloning of vaccine: Codon optimization of the vaccine's sequences facilitated successful cloning into a plasmid vector, an essential step for producing the vaccine in laboratory settings.

Supplementary data

Supplementary data is available at *Briefings in Bioinformatics* online.

Acknowledgements

The authors would like to express their heartfelt gratitude to Khwaja Yunus Ali University, as well as the Department of Biochemistry and Biotechnology, for providing the opportunity to conduct the research. The ultimate decision to submit the research for publication rested with the corresponding author, who had complete access to all of the research's information.

Author contributions

Mohammad Shahangir Biswas (Conceptualization, Data curation, Formal analysis, Investigation, Methodology, Project administration, Resources, Supervision, Validation, Visualization, Writing—original draft, Writing—review & editing), Suronjit Kumar Roy (Data curation, Formal analysis, Investigation, Methodology, Writing—review & editing), Foyzur Rahman (Writing—review & editing), Rubait Hasan (Writing—review & editing), Zahidur Rahmann (Writing—review & editing), and Md Moyen Uddin PK (Writing—review & editing).

Funding

None declared.

Conflict of interest: None declared.

Data availability

All authors have read and approved the final version of the manuscript. The corresponding author had full access to all of the data in this study and takes complete responsibility for the integrity of the data and the accuracy of the data analysis.

Ethics statement

There is nothing new to report from the authors.

Transparency statement

The lead author M.S.B. affirms that this manuscript is an honest, accurate, and transparent account of the study being reported; that no important aspects of the study have been omitted; and that any discrepancies from the study as planned (and, if relevant, registered) have been explained.

References

1. Founou RC, Founou LL, Essack SY. Clinical and economic impact of antibiotic resistance in developing countries: a systematic review and meta-analysis. *Plos One* 2017;**12**:e0189621. https://doi.org/10.1371/journal.pone.0189621.
2. Mulani MS, Kamble EE, Kumkar SN. *et al.* Emerging strategies to combat ESKAPE pathogens in the era of antimicrobial resistance: a review. *Front Microbiol* 2019;**10**:403107. https://doi.org/10.3389/fmicb.2019.00539.

3. Tacconelli E, Carrara E, Savoldi A. *et al.* Articles discovery, research, and development of new antibiotics: the WHO priority list of antibiotic-resistant bacteria and tuberculosis. *Lancet Infect Dis* 2018;**18**:318–27.
4. Bereanu A-S, Bereanu R, Mohor C. *et al.* Prevalence of infections and antimicrobial resistance of ESKAPE group bacteria isolated from patients admitted to the intensive care unit of a county emergency hospital in Romania. *Antibiotics* 2024;**13**:400. https://doi.org/10.3390/antibiotics13050400.
5. Wood SJ, Kuzel TM, Shafikhani SH. Pseudomonas aeruginosa: infections, animal modeling, and therapeutics. *Cells* 2023;**12**:199. https://doi.org/10.3390/cells12010199.
6. Qin S, Xiao W, Zhou C. *et al.* Pseudomonas aeruginosa: pathogenesis, virulence factors, antibiotic resistance, interaction with host, technology advances and emerging therapeutics. *Signal Transduct Target Ther* 2022;**7**:199. https://doi.org/10.1038/s41392-022-01056-1.
7. WHO Bacterial Priority Pathogens List, 2024: bacterial pathogens of public healthimportance to guide research, development and strategies to prevent and control antimicrobial resistance. Geneva: World Health Organization; 2024. Available from: https://www.doherty.edu.au/news-events/news/who-global-priority-pathogens-list-of-antibiotic-resistant-bacteria.
8. Klockgether J, Cramer N, Wiehlmann L. *et al.* Pseudomonas aeruginosa genomic structure and diversity. *Front Microbiol* **2**:150. https://doi.org/10.3389/fmicb.2011.00150.
9. Sharma S, Mohler J, Mahajan SD. *et al.* Microbial biofilm: a review on formation, infection, antibiotic resistance, control measures, and innovative treatment. *Microorganisms* 2023;**11**:1614. https://doi.org/10.3390/microorganisms11061614.
10. Başkan C, Yıldırım T, Bilgin M. *et al.* Determination of biofilm formation, antibiotic susceptibility profiles and quorum sensing mediated virulence factors in ceftazidime resistant Pseudomonas aeruginosa. *Biologia* 2023;**78**:2881–93. https://doi.org/10.1007/s11756-023-01429-z.
11. Silva A, Silva V, López M. *et al.* Antimicrobial resistance, genetic lineages, and biofilm formation in Pseudomonas aeruginosa isolated from human infections: an emerging one health concern. *Antibiotics (Basel)* 2023;**12**:1248. https://doi.org/10.3390/antibiotics12081248.
12. Hentzer M, Teitzel GM, Balzer GJ. *et al.* Alginate overproduction affects Pseudomonas aeruginosa biofilm structure and function. *J Bacteriol* 2001;**183**:5395–401. https://doi.org/10.1128/JB.183.18.5395-5401.2001.
13. Wood SJ, Goldufsky JW, Seu MY. *et al.* Pseudomonas aeruginosa cytotoxins: mechanisms of cytotoxicity and impact on inflammatory responses. *Cells* 2023;**12**:195. https://doi.org/10.3390/cells12010195.
14. Yaeger LN, Ranieri MR, Chee J. *et al.* A genetic screen identifies a role for oprF in Pseudomonas aeruginosa biofilm stimulation by subinhibitory antibiotics. *NPJ Biofilms Microbiomes* 2024;**10**:1–12. https://doi.org/10.1038/s41522-024-00496-7.
15. Lin YM, Wu SJ, Chang TW. *et al.* Outer membrane protein I of Pseudomonas aeruginosa is a target of cationic antimicrobial peptide/protein. *J Biol Chem* 2010;**285**:8985–94. https://doi.org/10.1074/jbc.M109.078725.
16. Ude J, Tripathi V, Buyck JM. *et al.* Outer membrane permeability: antimicrobials and diverse nutrients bypass porins in Pseudomonas aeruginosa. *Proc Natl Acad Sci U S A* 2021;**118**:e2107644118. https://doi.org/10.1073/pnas.2107644118.
17. Barone S, Mateu B, Turco L. *et al.* Unveiling the modulation of Pseudomonas aeruginosa virulence and biofilm formation by selective histone deacetylase 6 inhibitors. *Front Microbiol* 2024;**15**:1340585. https://doi.org/10.3389/fmicb.2024.1340585.
18. Hussein EF. Pseudomonas aeruginosa Represents a Main Cause of Hospital-Acquired Infections (HAI) and Multidrug Resistance (MDR) [Internet]. Pseudomonas aeruginosa: New Perspectives and Applications. IntechOpen, 2024, London, UK. Available from: https://dx.doi.org/10.577/intechopen.108759.
19. Sathe N, Beech P, Croft L. *et al.* Pseudomonas aeruginosa: infections and novel approaches to treatment "knowing the enemy" the threat of Pseudomonas aeruginosa and exploring novel approaches to treatment. *Inf Med* 2023;**2**:178–94. https://doi.org/10.1016/j.imj.2023.05.003.
20. Sievert DM, Ricks P, Edwards JR. *et al.* Antimicrobial-resistant pathogens associated with healthcare-associated infections: summary of data reported to the National Healthcare Safety Network at the Centers for Disease Control and Prevention, 2009-2010. *Infect Control Hosp Epidemiol* 2013;**34**:1–14. https://doi.org/10.1086/668770.
21. Weber DJ, Rutala WA, Sickbert-Bennett EE. *et al.* Microbiology of ventilator–associated pneumonia compared with that of hospital-acquired pneumonia. *Infect Control Hosp Epidemiol* 2007;**28**:825–31. https://doi.org/10.1086/518460.
22. Weiner LM, Webb AK, Limbago B. *et al.* Antimicrobial-resistant pathogens associated with healthcare-associated infections: summary of data reported to the National Healthcare Safety Network at the Centers for Disease Control and Prevention, 2011-2014. *Infect Control Hosp Epidemiol* 2016;**37**:1288–301. https://doi.org/10.1017/ice.2016.174.
23. *Patient Registry | Cystic Fibrosis Foundation*. Bethesda, Maryland. https://www.cff.org/medical-professionals/patient-registry
24. Murray CK, Wilkins K, Molter NC. *et al.* Infections complicating the care of combat casualties during operations Iraqi Freedom and Enduring Freedom. *J Trauma* 2011;**71**:S62–73. https://doi.org/10.1097/TA.0b013e3182218c99.
25. Tribble DR, Li P, Warkentien TE. *et al.* Impact of operational theater on combat and noncombat trauma-related infections. *Mil Med* 2016;**181**:1258–68. https://doi.org/10.7205/MILMED-D-15-00368.
26. Chatzinikolaou I, Abi-Said D, Bodey GP. *et al.* Recent experience with Pseudomonas aeruginosa bacteremia in patients with cancer: retrospective analysis of 245 episodes. *Arch Intern Med* 2000;**160**:501–9. https://doi.org/10.1001/archinte.160.4.501.
27. Baker SM, McLachlan JB, Morici LA. Immunological considerations in the development of Pseudomonas aeruginosa vaccines. *Hum Vaccin Immunother* 2020;**16**:412–8. https://doi.org/10.1080/21645515.2019.1650999.
28. Cleland H, Tracy LM, Padiglione A. *et al.* Patterns of multidrug resistant organism acquisition in an adult specialist burns service: a retrospective review. *Antimicrob Resist Infect Control* 2022;**11**:82. https://doi.org/10.1186/s13756-022-01123-w.
29. Fournier A, Eggimann P, Pantet O. *et al.* Antibiotics' consumption to early detect epidemics of P. aeruginosa in a burn center: a paradigm shift in the epidemiological surveillance of nosocomial infections. *Antimicrob Resist Infect Control* 2015;**4**:P232.
30. Decraene V, Ghebrehewet S, Dardamissis E. *et al.* An outbreak of multidrug-resistant Pseudomonas aeruginosa in a burns service in the north of England: challenges of infection prevention and control in a complex setting. *J Hosp Infect* 2018;**100**:e239–45. https://doi.org/10.1016/j.jhin.2018.07.012.
31. Artimo P, Jonnalagedda M, Arnold K. *et al.* ExPASy: SIB bioinformatics resource portal. *Nucleic Acids Res* 2012;**40**:W597–603. https://doi.org/10.1093/nar/gks400.

32. Doytchinova IA, Flower DR. VaxiJen: a server for prediction of protective antigens, tumour antigens and subunit vaccines. *BMC bioinformatics* 2007;**8**:1–7.
33. Jespersen MC, Peters B, Nielsen M. *et al.* BepiPred-2.0: improving sequence-based B-cell epitope prediction using conformational epitopes. *Nucleic Acids Res* 2017;**45**:W24–9. https://doi.org/10.1093/nar/gkx346.
34. Kim Y, Ponomarenko J, Zhu Z. *et al.* Immune epitope database analysis resource. *Nucleic Acids Res* 2012;**40**:W525–30. https://doi.org/10.1093/nar/gks438.
35. Vita R, Overton JA, Greenbaum JA. *et al.* The immune epitope database (IEDB) 3.0. *Nucleic Acids Res* 2015;**43**:D405–12. https://doi.org/10.1093/nar/gku938.
36. Thomsen M, Lundegaard C, Buus S. *et al.* MHCcluster, a method for functional clustering of MHC molecules. *Immunogenetics* 2013;**65**:655–65. https://doi.org/10.1007/s00251-013-0714-9.
37. Nielsen M, Lundegaard C, Lund O. Prediction of MHC class II binding affinity using SMM-align, a novel stabilization matrix alignment method. *BMC Bioinformatics.* 2007;**8**:1–12. https://doi.org/10.1186/1471-2105-8-238.
38. Peters B, Sette A. Generating quantitative models describing the sequence specificity of biological processes with the stabilized matrix method. *BMC Bioinformatics* 2005;**6**:1–9. https://doi.org/10.1186/1471-2105-6-132.
39. Dey J, Mahapatra SR, Patnaik S. *et al.* Molecular characterization and designing of a novel multiepitope vaccine construct against Pseudomonas aeruginosa. *Int J Pept Res Ther* 2022;**28**:1–19. https://doi.org/10.1007/s10989-021-10356-z.
40. Dimitrov I, Bangov I, Flower DR. *et al.* AllerTOP v.2—a server for in silico prediction of allergens. *J Mol Model* 2014;**20**:2278. https://doi.org/10.1007/s00894-014-2278-5.
41. Gupta S, Kapoor P, Chaudhary K. *et al.* In silico approach for predicting toxicity of peptides and proteins. *PloS One* 2013;**8**:e73957. https://doi.org/10.1371/journal.pone.0073957.
42. Saadi M, Karkhah A, Nouri HR. Development of a multi-epitope peptide vaccine inducing robust T cell responses against brucellosis using immunoinformatics based approaches. *Infect Genet Evol* 2017;**51**:227–34. https://doi.org/10.1016/j.meegid.2017.04.009.
43. Arai R, Ueda H, Kitayama A. *et al.* Design of the linkers which effectively separate domains of a bifunctional fusion protein. *Protein Eng* 2001;**14**:529–32. https://doi.org/10.1093/protein/14.8.529.
44. Li X, Xing Y, Guo L. *et al.* Oral immunization with recombinant Lactococcus lactis delivering a multi-epitope antigen CTB-UE attenuates Helicobacter pylori infection in mice. *Pathog Dis* 2014;**72**:78–86. https://doi.org/10.1111/2049-632X.12173.
45. Albekairi TH, Alshammari A, Alharbi M. *et al.* Design of a multi-epitope vaccine against Tropheryma whipplei using immunoinformatics and molecular dynamics simulation techniques. *Vaccine* 2022;**10**:691. https://doi.org/10.3390/vaccines10050691.
46. Bui HH, Sidney J, Dinh K. *et al.* Predicting population coverage of T-cell epitope-based diagnostics and vaccines. *BMC Bioinformatics* 2006;**7**:1–5. https://doi.org/10.1186/1471-2105-7-153.
47. Rapin N, Lund O, Bernaschi M. *et al.* Computational immunology meets bioinformatics: the use of prediction tools for molecular binding in the simulation of the immune system. *PloS One* 2010;**5**:1–14, e9862. https://doi.org/10.1371/journal.pone.0009862.
48. Grote A, Hiller K, Scheer M. *et al.* JCat: a novel tool to adapt codon usage of a target gene to its potential expression host. *Nucleic Acids Res* 2005;**33**:W526–31. https://doi.org/10.1093/nar/gki376.
49. Motamedi H, Alvandi A, Fathollahi M. *et al.* In silico designing and immunoinformatics analysis of a novel peptide vaccine against metallo-beta-lactamase (VIM and IMP) variants. *PloS One* 2023;**18**:e0275237. https://doi.org/10.1371/journal.pone.0275237.
50. Zhou HQ, Ning LW, Zhang HX. *et al.* Analysis of the relationship between genomic GC content and patterns of base usage, codon usage and amino acid usage in prokaryotes: similar GC content adopts similar compositional frequencies regardless of the phylogenetic lineages. *PloS One* 2014;**9**:1–7, e107319. https://doi.org/10.1371/journal.pone.0107319.
51. Motta S, Vecchietti D, Martorana AM. *et al.* The landscape of Pseudomonas aeruginosa membrane-associated proteins. *Cells* 2020;**9**:1–17. https://doi.org/10.3390/cells9112421.
52. Irum S, Andleeb S, Ali A. *et al.* Quest for novel preventive and therapeutic options against multidrug-resistant Pseudomonas aeruginosa. *Int J Pept Res Ther* 2021;**27**:2313–31. https://doi.org/10.1007/s10989-021-10255-3.
53. Chakraborty C, Sharma AR, Bhattacharya M. *et al.* Immunoinformatics approach for the identification and characterization of T cell and B cell epitopes towards the peptide-based vaccine against SARS-CoV-2. *Arch Med Res* 2021;**52**:362–70. https://doi.org/10.1016/j.arcmed.2021.01.004.
54. Terry FE, Moise L, Martin RF. *et al.* Time for T? Immunoinformatics addresses vaccine design for neglected tropical and emerging infectious diseases. *Expert Rev Vaccines* 2015;**14**:21–35. https://doi.org/10.1586/14760584.2015.955478.
55. Oli AN, Obialor WO, Ositadimma M. *et al.* Immunoinformatics and vaccine development: an overview. *Immunotargets Ther* 2020;**9**:13–30. https://doi.org/10.2147/ITT.S241064.
56. Jalal K, Khan K, Basharat Z. *et al.* Reverse vaccinology approach for multi-epitope centered vaccine design against delta variant of the SARS-CoV-2. *Environ Sci Pollut Res* 2022;**29**:60035–53. https://doi.org/10.1007/s11356-022-19979-1.
57. Holmgren J, Adamsson J, Anjuère F. *et al.* Mucosal adjuvants and anti-infection and anti-immunopathology vaccines based on cholera toxin, cholera toxin B subunit and CpG DNA. *Immunol Lett* 2005;**97**:181–8. https://doi.org/10.1016/j.imlet.2004.11.009.
58. Solomon JS, Nixon CP, McGarvey ST. *et al.* Expression, purification, and human antibody response to a 67 kDa vaccine candidate for Schistosomiasis japonica. *Protein Expr Purif* 2004;**36**:226–31. https://doi.org/10.1016/j.pep.2004.04.011.
59. Brandau DT, Jones LS, Wiethoff CM, Rexroad J, Middaugh CR. Thermal stability of vaccines. *Journal of Pharmaceutical Sciences* 2003;**92**:218–31.
60. Gasteiger E, Hoogland C, Gattiker A. *et al.* Protein identification and analysis tools on the ExPASy server. *The Proteomics Protocols Handbook*. Springer Protocols Handbooks. Humana Press. 2005; 571–607. https://doi.org/10.1385/1-59259-890-0:571.
61. Oladipo EK, Ajayi AF, Onile OS. *et al.* Designing a conserved peptide-based subunit vaccine against SARS-CoV-2 using immunoinformatics approach. *In Silico Pharmacol* 2021;**9**:1–21.
62. Heo L, Park H, Seok C. GalaxyRefine: protein structure refinement driven by side-chain repacking. *Nucleic Acids Res* 2013;**41**:W384–8. https://doi.org/10.1093/nar/gkt458.
63. Agnihotry S, Pathak RK, Singh DB. *et al.* Protein structure prediction. *Bioinformatics*. Elsevier, 2022;**7**:177–88. https://doi.org/10.1016/B978-0-323-89775-4.00023-7.
64. Kalita J, Padhi AK, Tripathi T. Designing a vaccine for fascioliasis using immunogenic 24 kDa mu-class glutathione s-transferase. *Infect Genet Evol* 2020;**83**:104352. https://doi.org/10.1016/j.meegid.2020.104352.
65. Qamar MTU, Shokat Z, Muneer I. *et al.* Multiepitope-based subunit vaccine design and evaluation against respiratory syncytial virus using reverse vaccinology approach. *Vaccines (Basel)* 2020;**8**:1–27.

66. Kufera JT, Armstrong C, Wu F. *et al.* CD4+ T cells with latent HIV-1 have reduced proliferative responses to T cell receptor stimulation. *J Exp Med* 2024;**221**:1–18. https://doi.org/10.1084/jem.20231511.
67. Apcher S, Prado Martins R, Fåhraeus R. The source of MHC class I presented peptides and its implications. *Curr Opin Immunol* 2016;**40**:117–22. https://doi.org/10.1016/j.coi.2016.04.002.
68. Germain RN. MHC-dependent antigen processing and peptide presentation: providing ligands for T lymphocyte activation. *Cell* 1994;**76**:287–99. https://doi.org/10.1016/0092-8674(94)90336-0.
69. Aiman S, Alhamhoom Y, Ali F. *et al.* Multi-epitope chimeric vaccine design against emerging Monkeypox virus via reverse vaccinology techniques- a bioinformatics and immunoinformatics approach. *Front Immunol* 2022;**13**:985450. https://doi.org/10.3389/fimmu.2022.985450.
70. Zhu F, Tan C, Li C. *et al.* Design of a multi-epitope vaccine against six Nocardia species based on reverse vaccinology combined with immunoinformatics. *Front Immunol* 2023;**14**:1100188. https://doi.org/10.3389/fimmu.2023.1100188.
71. Soltan MA, Abdulsahib WK, Amer M. *et al.* Mining of Marburg Virus Proteome for designing an epitope-based vaccine. *Front Immunol* 2022;**13**:13. https://doi.org/10.3389/fimmu.2022.907481.
72. Al-Karmalawy AA, Dahab MA, Metwaly AM. *et al.* Molecular docking and dynamics simulation revealed the potential inhibitory activity of ACEIs against SARS-CoV-2 targeting the hACE2 receptor. *Front Chem* 2021;**9**:9. https://doi.org/10.3389/fchem.2021.661230.
73. Soltan MA, Behairy MY, Abdelkader MS. *et al.* In silico designing of an epitope-based vaccine against common E. coli pathotypes. *Front Med (Lausanne)* 2022;**9**:829467. https://doi.org/10.3389/fmed.2022.829467.
74. Ragone C, Manolio C, Cavalluzzo B. *et al.* Identification and validation of viral antigens sharing sequence and structural homology with tumor-associated antigens (TAAs). *J Immunother Cancer* 2021;**9**:e002694. https://doi.org/10.1136/jitc-2021-002694.
75. Rosano GL, Ceccarelli EA. Recombinant protein expression in Escherichia coli: advances and challenges. *Front Microbiol* 2014;**5**:5(APR). https://doi.org/10.3389/fmicb.2014.00172.
76. Chen R. Bacterial expression systems for recombinant protein production: E. coli and beyond. *Biotechnology Advances*, 2012;**30**:1102–1107. https://doi.org/10.1016/j.biotechadv.2011.09.013.